



Carbon Nanotube Yarn Actuators: An Electrochemical Impedance Model

Tissaphern Mirfakhrai,^{a,*} Jiyoung Oh,^b Mikhail Kozlov,^b Shaoli Fang,^b
Mei Zhang,^b Ray H. Baughman,^b and John D. W. Madden^a

^aDepartment of Electrical and Computer Engineering, University of British Columbia, Vancouver BC, Canada V6T 1Z4

^bAlan G. MacDiarmid NanoTech Institute, University of Texas at Dallas, Richardson, Texas 75080, USA

Twist-spun yarns made of carbon nanotubes have been shown to work as electrochemical actuators and force sensors. The electrochemical response of these yarns at different bias potentials was studied using electrochemical impedance spectroscopy (EIS) and compared with results from cyclic voltammetry. Based on the EIS results, the capacitance is estimated first by directly fitting a resistance–capacitance circuit and then by fitting a circuit including a constant phase element (CPE), estimating the capacitance based on the CPE. The gravimetric capacitance in aqueous electrolyte is found to be about 12 F/g and relatively independent of bias, while in an acetonitrile-based electrolyte it is a function of the bias potential, increasing to nearly 20 F/g when the bias potential is larger. The capacitance per unit surface area of the multiwalled nanotubes bundles in the yarn is estimated to be about 0.05 F/m².

© 2009 The Electrochemical Society. [DOI: 10.1149/1.3106048] All rights reserved.

Manuscript submitted October 8, 2008; revised manuscript received December 24, 2008. Published April 6, 2009.

Individual carbon nanotubes (CNTs) have been shown to have high modulus (0.7 TPa) and high strength (30 GPa) while also displaying high electrical (10–30 kS/cm) and thermal (2000 W/mK) conductivities.¹ The low density of CNTs makes their gravimetric properties even more useful, hence the interest of technologists in developing applications. Commercial applications have been delayed by the absence of methods for controlling the arrangement of typically over a trillion CNTs as they are being assembled into fibers and textiles and accomplishing this assembly at industrially useful rates.

A recently demonstrated assembly method is to create twist-spun yarns of multiwalled nanotubes (MWNTs) by drawing yarns from aligned forests of nanotubes.² A scanning electron micrograph of such a yarn is shown in Fig. 1a. The MWNTs in these yarns are held together by the combination of twist-based lateral forces and van der Waals interactions between bundled nanotubes, whose effect is enhanced by long MWNT lengths and incorporation of individual MWNTs in more than one bundle. We have previously shown that a dimensional change takes place in the yarns when a voltage is applied to them in an electrolyte.³ Due to the high tensile strength (1 GPa) and Young's modulus (20 GPa) of the yarns,⁴ the yarns can operate under high loads to produce useful work output. Like many other actuators, they can also operate in reverse to convert mechanical energy to electrical energy, thereby acting as mechanical force sensors and electrical energy generators.^{5,6}

Both actuation and sensing effects are most evident when the yarn is used as an electrode in an electrochemical cell and is thus electrochemically charged. This means that in order to fully characterize the yarn as an actuator and sensor, its electrochemical behavior needs to be studied. A number of works have used electrochemical impedance spectroscopy (EIS) to characterize the electrochemical behavior of CNTs. Yang and Wu⁷ compared the EIS response of capped and uncapped CNTs created by arc discharge. They used a nonaqueous electrolyte and reported a difference between the response of open- and closed-ended CNTs. Yang et al.⁸ attempted to fit a circuit model to the EIS data of a mixture of MWNTs, carbon black, and polyvinylidene fluoride and to relate the changes in the values of the circuit-model parameters to the variations of the diffusion constants with applied bias. Zhang et al.⁹ compared the EIS response of entangled CNTs with that of aligned CNT arrays and found a lower series resistance and higher gravimetric capacitance for the aligned CNT arrays. Liu et al.¹⁰ studied the

effect of electrochemical oxidation on the EIS response of CNTs. They used the EIS data to show that the oxidative purification treatments on CNTs open their ends, shorten their lengths, make defects on the tube walls, and therefore enlarge their specific surface area. Therefore, the electrical double-layer capacitance of the CNTs is greatly increased. Barisci et al.¹¹ used EIS to study and model sheets of Bucky paper and also to fit a circuit model. They showed that both the effective capacitance and electrode resistance were functions of the oxidation state of the Bucky paper. All these studies show the usefulness of using EIS in studying the electrochemical properties of nanotube-based structures and the application of circuit models to gain a better understanding of the electrochemical processes involved.

A close-up image of the yarn surface (Fig. 1b) shows that there are large gaps between the constituent MWNTs in the yarn and that the yarn surface is rough on a nanoscopic scale. This means that models for rough and porous electrode geometries may be needed to account for the electrochemical behavior of the yarn. In this paper, we employ EIS and cyclic voltammetry (CV) to characterize the yarn. In the sections that follow, we first present the theoretical background needed to analyze the EIS data and to model the electrochemical behavior of the yarns and then present the experimental results and discussion.

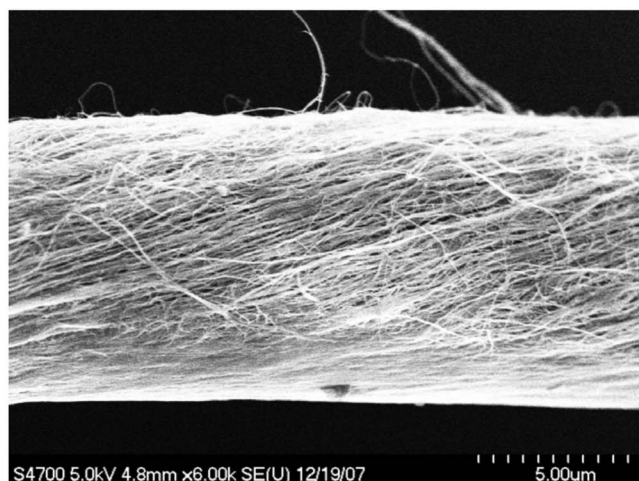
Theory

EIS can be used to study many electrochemical phenomena. Circuit models having a similar response to that of the electrochemical cell under study are often employed to relate the EIS behavior to physical phenomena. In many electrochemical applications, the values of the circuit parameters in such models are of prime importance in understanding the system. For example, in energy-storage devices, the capacitance of the electrode surface is the main quantity of interest, which can be estimated using EIS. EIS data is used to better understand corrosion¹² and to estimate the thickness of an electrochemically deposited layer.¹³ Because the actuation of the yarns depends on the charge stored in them,³ EIS may be a useful tool to study their behavior. Because of the porous structure of our yarns, we concentrate our discussion on the information that can be obtained from EIS data for porous electrodes.

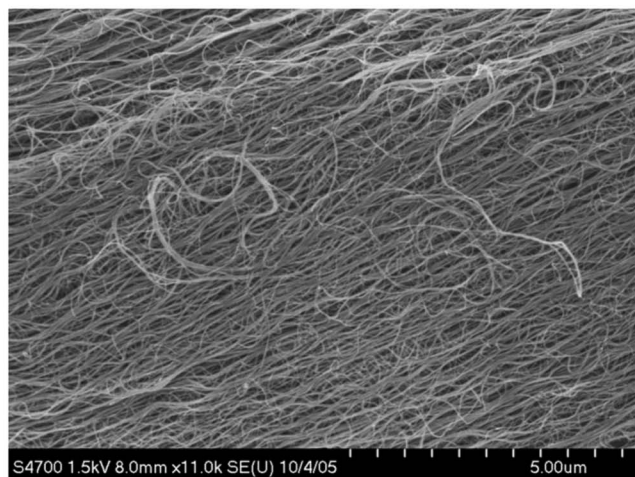
EIS of porous materials.—Porosity or roughness of the electrode surface is expected to change the frequency dependence of the interfacial impedance. A simple approach to the problem of porous and rough interfaces is based on the use of transmission line analogies.¹⁴ Consider a cylindrical pore in a conducting electrode as depicted in Fig. 2. If the series resistance of the electrolyte per unit

* Electrochemical Society Student Member.

^z E-mail: tissa@ece.ubc.ca



(a)



(b)

Figure 1. Scanning electron micrographs of (a) a twist-spun CNT yarn and (b) a close-up of the yarn surface, showing individual MWNTs and MWNT bundles.

length is R_0 , and the interfacial capacitance per unit length is C_0 , then the pore behaves as a transmission line and has an impedance given by

$$Z = \sqrt{\frac{R_0}{j\omega C_0}} \quad [1]$$

where $j = \sqrt{-1}$, $\omega = 2\pi f$, and f is the frequency of the electrical excitation.

A derivation of Eq. 1 can be found in the Appendix. This approach can be extended to more complex situations that include

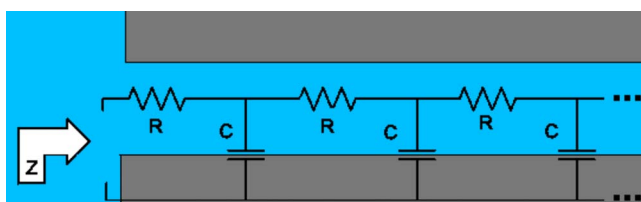


Figure 2. (Color online) A narrow pore in a porous conducting electrode.

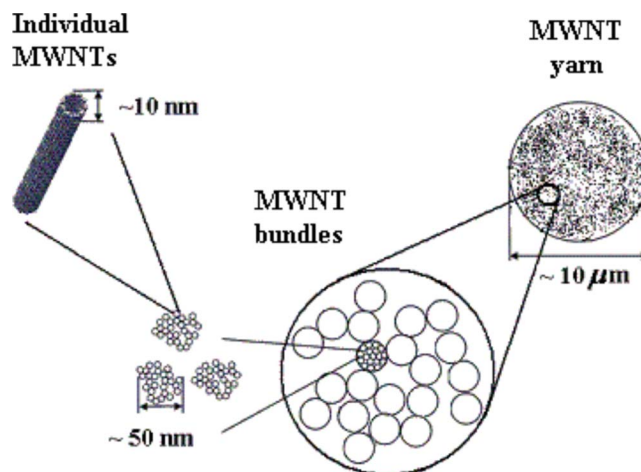


Figure 3. (Color online) The nested fractal structure of twist-spun MWNT yarns.

pores of finite depth, nonuniform pores, and situations where the interfacial capacitance is replaced by a complex admittance, corresponding to electrochemical reactions taking place down the depth of the pore.¹⁵ It is also possible to include finite electrode resistance.

In practice, the frequency dependence of the electrochemical response is often neither purely capacitive nor proportional to $1/\sqrt{j\omega}$. More generally, the impedance can take the form of

$$Z = \frac{1}{Y_0(j\omega)^P} \quad [2]$$

where P is a real number, usually close to unity.¹⁵ Depending on the structure of the porous electrode, the value of P may vary. Y_0 is a constant combining the resistive and capacitive properties of the electrode. If Y_0 is a real number, the impedance, Z , has a constant phase angle. Therefore, it is known as a constant phase element (CPE). Y_0 can be related to the thickness of the double layer, because it includes the effect of the size of the double-layer capacitance.

Some attempts have been made in relating the parameters of a CPE model to the electrode properties and geometry. Le Mehaute^{16,17} represented a rough or porous electrode–electrolyte interface as a fractal and proposed that the exponent P of the CPE is related to the fractal dimension D . Sapoval and Chazalviel studied cases where faradaic and diffusion processes coexist in fractal electrodes. They proposed a number of equivalent circuit networks for particular fractal geometries and suggested a relationship between the fractal dimension and the model network parameters.¹⁸ Scheider showed how almost any arbitrary value of exponent P can be modeled by replacing some branches in the circuit in Fig. 2 with transmission lines themselves.¹⁹ He also presented an argument in an attempt to relate the branched network configurations to the physical realities of the electrode–electrolyte interface.

In the case of our yarns, individual MWNTs having diameters of about 10 nm form into more or less cylindrical bundles that have diameters ranging from 50 to 100 nm. Combinations of these bundles form the twisted yarn, which is again cylindrical. It can therefore be approximated that the yarn is formed of nested self-similar objects of variable dimensions and can qualify as a “fractal” electrode (Fig. 3). Thus, it is not unexpected if the impedance of the yarn behaves like a CPE. However, proof of existence of a universal relationship between the fractal dimension and the CPE parameters, as well as its exact form and quantitative nature, are subjects open to investigation.^{18,20}

A parallel way of studying the impedance behavior of the yarn is to consider diffusion and field effects, which can both contribute to the charging process of an electrode–electrolyte interface. For planar

electrodes, diffusion gradients are perpendicular to the electrode surface and opposed to the field direction. However, on a rough surface, like that of our yarns, roughness can cause uneven charging of the double layer. In such situations, considerable diffusion gradients tangential to the electrode surface may exist.¹⁹ The relative magnitude of the charge moving due to the lateral diffusion gradients compared to the charge moving in the direction of the electric field depends on the radius of curvature and the roughness of the surface.

As discussed in Ref. 19, let us visualize diffusion over the surface of a MWNT bundle near the yarn surface. Figure 4 shows what happens to bundles of MWNTs in the yarn when a potential is applied to the yarn. Red spheres represent ions of opposite charge to the charge accumulated on the MWNT bundle surface, and (smaller) blue spheres represent ions with the same charge type as on the MWNTs. Imagine that a step in galvanostatic current is applied at $t = 0$. Initially, no concentration gradients are present, and ions (red spheres in Fig. 4) flow along the electric field lines (Fig. 4a) to the exposed side of the MWNT bundle. As charge accumulates in the double layer on the exposed side of the bundle, the folding down of the equipotential lines and the lateral concentration gradient cause tangential spreading of ions to the space around the bundle (Fig. 4b). The line of constant electric potential (Φ) moves closer and folds around the bundle peak. At the peak, the concentration gradient vector N opposes the electric field, while at the side the concentration gradient has a tangential component which acts in the same direction as the electric field. As time passes, larger parts of the surface become accessible to charge, and the effective capacitance increases.

To estimate the orders of magnitude involved in this process, it can be supposed that an artificial boundary B may be drawn (see Fig. 4c) dividing the surface into the exposed side, A, and a valley side, C. The exposed side, A, (see Fig. 4c) is assumed to charge uniformly as if it were a segment of a perfectly smooth parallel plane electrode, while the valley side C is assumed to be completely shielded from the bulk electrolyte. The double layer in the valley is thus charged exclusively from the input at B by ions moving under the lateral electrodiffusion potential gradient. This movement along the surface C is described mathematically by the branched network shown. This branched network forms a first-order series-series network, with another resistance-capacitance (RC) ladder formed along the length of the yarn due to the surface capacitance and the resistance along the length of the MWNT bundles and the resistance of the electrolyte (Fig. 4d). It is assumed that the ladder circuits along the length of the MWNT bundles are connected together at the ends of the yarn. Scheider¹⁹ showed that the frequency response of such a first-order series-series branched RC ladder network corresponds to a phase exponent of 0.75. He also showed that including a third level of branching in the circuit model can lead a CPE exponent of 0.875. We shall use this theory to compare the frequency response of the MWNT yarns with that of a CPE and to find a circuit model employing a CPE for the MWNT yarn electrode.

Finding the equivalent capacitance of a CPE.— It is often desirable to have an estimate of the “capacitance” of an electrode surface. Because the actuation of the MWNT yarns depends on the charge stored in them, it is useful to find an estimate of their capacitance. One way of finding such a capacitance is to fit an RC circuit model to the impedance of the cell. However, if such a fit is not good, the value of the capacitance obtained this way may not be useful. Several attempts have been made to find the capacitance of a CPE.²¹ Hsu and Mansfeld¹³ proposed a method to estimate the capacitance of a CPE. Their method is based on the fact that in a circuit consisting of a CPE in parallel with a resistor, the real part of the impedance becomes independent of the exponent P at the frequency where the imaginary part of the impedance has a maximum (ω_m). At that frequency, all the energy loss in the cell can be assumed to be in the resistor, and the CPE can be set equivalent to a capacitor. Based on Kramers–Kronig theorem, the resistance of the parallel resistor can then be calculated²² using

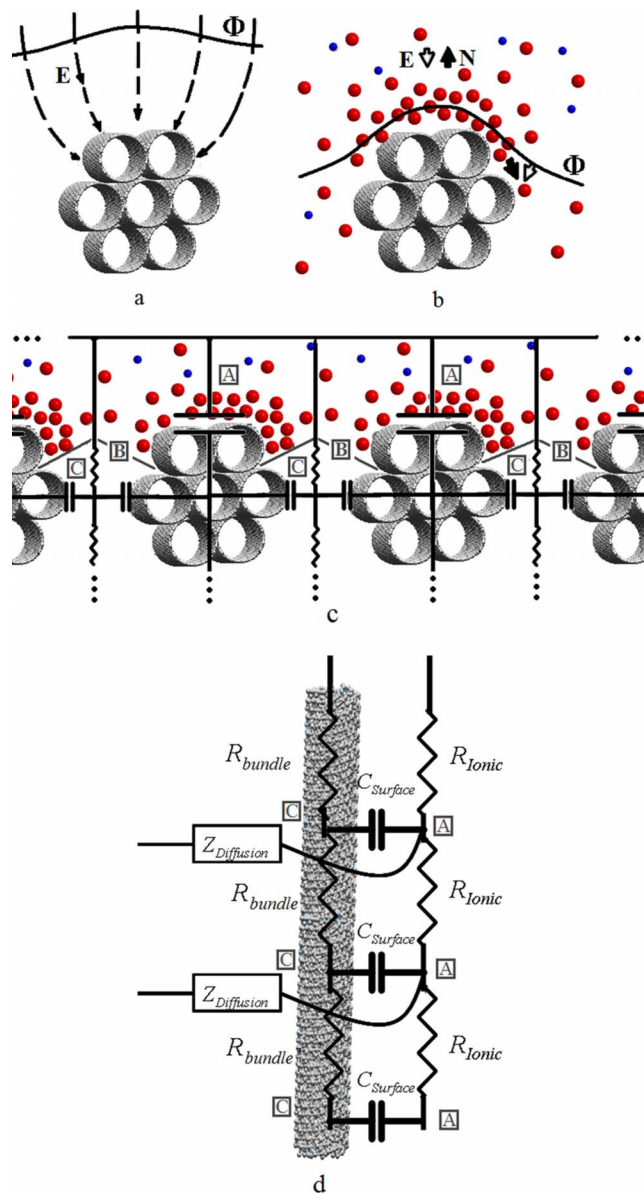


Figure 4. (Color online) Visualization of a MWNT bundle within the yarn. (a) Electric field lines E initially converge toward the exposed face of MWNT bundle, while the gaps around the bundle are partially shielded. (b) With accumulation of ions that follow the electric field lines to the outermost point of the bundle, a concentration gradient is established. (c) An artificial boundary B is drawn to visualize the process by which accumulated charge in the outer areas A spreads to the valley sides C under the force of the tangential electrodiffusion potential gradient. (d) The RC ladder circuit formed by the resistance of the MWNTs and the ionic resistance of the electrolyte along with the diffusion impedance into the yarn. Each $Z_{\text{Diffusion}}$ impedance block represents an RC ladder circuit similar to the one in Fig. 2. The drawn cylinder represents any of the bundles in c, and the capacitors labeled C_{Surface} are the same as the surface capacitances in c, this time drawn from a side angle.

$$R = 2.3 \times \frac{4}{\pi} \int_{\omega_m}^{\infty} Z''(\omega) d(\log \omega) \quad [3]$$

where Z'' is the imaginary part of the measured impedance. If Z'' varies monotonically with frequency, it has no clear maximum point, so Eq. 3 can only provide a lower limit for the resistance. Because the above equation is independent of the CPE exponent P , it also applies for a pure capacitor, which is a CPE with $P = 1$.

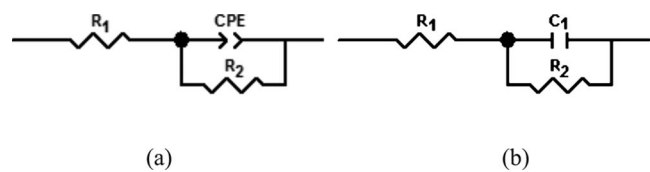


Figure 5. Proposed circuit models for the electrochemical behavior of the MWNT yarn electrode using (a) a CPE and (b) an ideal capacitor. The series resistor R_1 models the solution and contact resistance and the parallel resistor R_2 models the processes resulting in a loss of the stored charge.

Using the value of R from the above equation, the equivalent capacitance can be found as

$$C = \frac{1}{\omega_m R} \quad [4]$$

We use this equation to determine the capacitance of the CPE element representing the MWNT yarn and compare it with the capacitance value obtained from fitting a simple RC model to the same impedance response.

Experimental Results and Discussion

A twist-spun yarn of carbon nanotubes with a diameter of about 10 μm was used as the working electrode (WE) in an electrochemical cell. In the case of aqueous electrolyte, the length of the yarn immersed in the electrolyte was 15 mm, and in the case of acetonitrile, it was 5 mm. In both cases the yarn was held in place in the electrolyte using a Teflon clamp. The other end of the yarn was held outside the electrolyte where electronic contact was made to it. The yarn was otherwise exposed to the solution all around. Images and diagrams of the cell setup can be found in Ref. 3 and 23. The counter electrode (CE) was a piece of avCarb carbon fiber paper whose surface area was substantially larger than that of the yarn. The electrochemical impedance of the cell was measured in a 1 M aqueous solution of sodium hexafluorophosphate (NaPF_6), as well as in a 0.2 M solution of tetrabutylammonium hexafluorophosphate (TBAPF_6) in acetonitrile, at various bias potentials applied between the WE and CE. In the case of the aqueous electrolyte, the reference electrode (RE) was Ag/AgCl in 3 M NaCl, and in the case of the acetonitrile-based electrolyte, it was 0.1 M AgNO_3 in acetonitrile, hereby referred to as Ag/Ag $^+$. The impedance of the cell was measured over a range of frequencies spanning from 10 mHz to 10 kHz using a Solatron SI 1260 Impedance/Gain-Phase Analyzer equipped with an SI 1287 Electrochemical Interface. The amplitude of the ac signal was 20 mV in all cases. Data recording and fitting were performed using the ZView 3.0a software package with Calc-Modulus data weighing, which means each data point's weight is normalized by its magnitude during the fitting process. Cyclic voltammograms were also performed on both cells at a scan rate of 40 mV/s over the ranges of -1 to $+1$ V vs Ag/AgCl in 3 M NaCl in the aqueous electrolyte and -1.4 to $+0.6$ V vs Ag/Ag $^+$ in the acetonitrile-based electrolyte.

The impedance was found to have a real value at high frequencies. This is equivalent to a series resistance, which can be due to the solution and contact resistances. It was also found that as potential across the interface was increased to be substantially positive or negative, some parasitic reactions started occurring at the interface, which resulted in some charge being transmitted from the electrode to the ions in the electrolyte, thus effectively shunting the capacitor. It was therefore decided to model the cell impedance as a circuit consisting of a resistor in series with the parallel combination of a CPE and a resistor (Fig. 5a). The resistor R_1 represents the electrolyte and contact resistance, and R_2 represents the charge-transfer resistance across the interface, leading to partially discharging the capacitor. For comparison, an alternative circuit model was also used replacing the CPE with an ideal capacitor (Fig. 5b). Variations

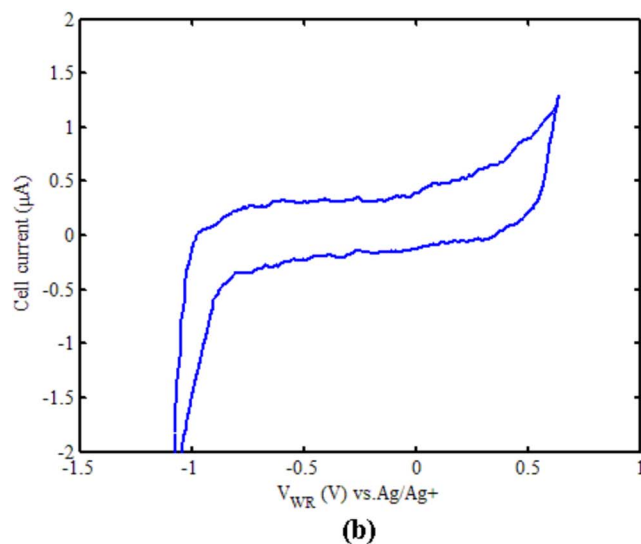
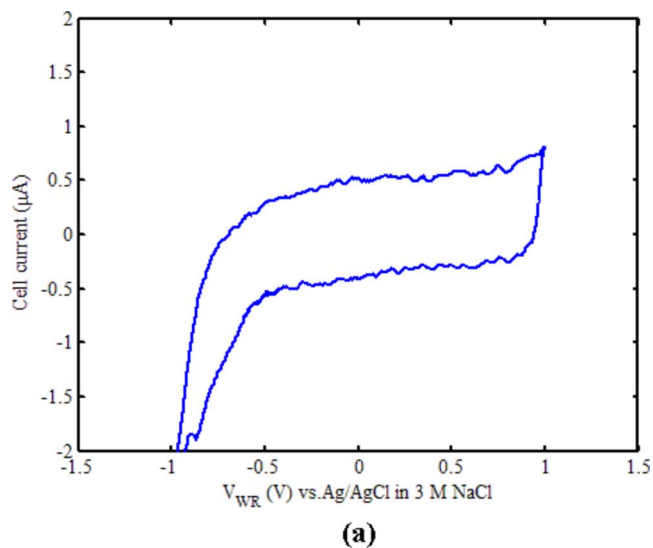


Figure 6. (Color online) Cyclic voltammograms of the yarn in (a) 1 M aqueous solution of NaPF_6 and (b) 0.2 M solution of TBAPF_6 in acetonitrile.

of these equivalent circuits were tested, but the best agreement with the experimental data was only observed when the proposed model was applied.

Experiments in aqueous NaPF_6 .— Figure 6a shows the CV results for the experiment in aqueous electrolyte. The results of the EIS measurements in a 1 M aqueous solution of NaPF_6 at various potentials ranging from -0.75 to $+1$ V vs RE are plotted in Fig. 7. The circuit in Fig. 5a was fitted to the impedance response, and the best-fit circuit parameter values are plotted as a function of the bias potential in Fig. 8. The simulated frequency responses of the best-fit circuits are shown as continuous lines along with the experimentally measured cell responses (dots) in Fig. 7. The error bars in Fig. 8b and c refer to the average error between the fit and the experimental data. The error in Fig. 8a is too small to be visible on the plot.

Figure 8c shows the dependence of the parallel resistor R_2 on the bias potential. At bias potentials close to 0 V, the value of the resistance R_2 becomes large and has little effect on the overall fitting error. This implies that this circuit parameter is unnecessary. The values for R_2 at those two points are therefore not shown in Fig. 8c. Looking at the CV plot (Fig. 6a), this behavior is expected, because almost no parasitic reactions should occur at low electrode potentials and therefore R_2 should act as open circuit at low potentials. As

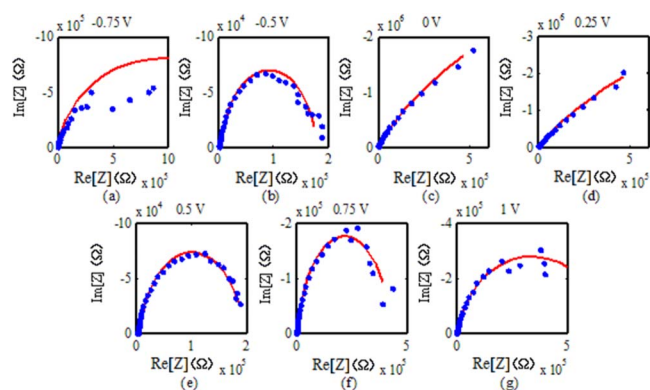


Figure 7. (Color online) Nyquist plots of the yarn impedance in a 1 M aqueous solution of NaPF_6 at various bias potentials: (a) -0.75 , (b) -0.5 , (c) 0 , (d) $+0.25$, (e) $+0.5$, (f) $+0.75$, and (g) 1 V vs Ag/AgCl in 3 M NaCl RE. The fit lines show the impedance response of the circuit model in Fig. 5a.

the potential is increased, the CV implies that parasitic reactions are substantial at potentials beyond $+0.8$ and below -0.5 V vs RE. This potential window of about 1.3 V is consistent with the electrolysis potentials of water, and therefore it is likely that the parasitic reactions, which increase as the potential limits are approached, are the result of decomposition of the water. The values of the parallel resistance R_2 from Eq. 3 are also plotted as a function of the applied bias potential (squares). As can be seen in Fig. 7c and d, at potentials close to zero, the impedance spectra are quite linear-looking, and therefore the imaginary part of the impedance does not reach a visible maximum as it does at other potentials. Therefore, Eq. 3 can only provide us with a lower limit on the resistance. This is consistent with the result of the direct fitting method, which predicted that R_2 was so large that the parallel resistor was found to be unnecessary. At other potentials, where the imaginary part of the impedance first increases and then decreases as the frequency is increased, ω_m can be found and R_2 can be calculated using Eq. 3. In Fig. 8c, the resistance values found in this way virtually coincide with those found using direct fitting. At higher potentials, R_2 becomes much

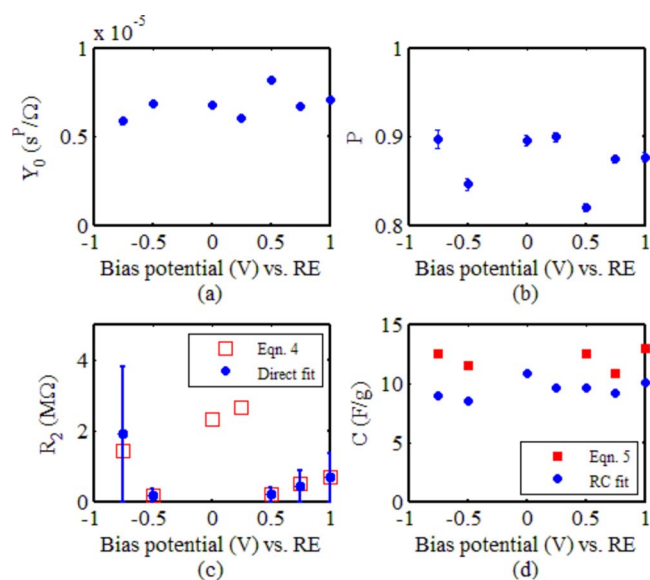


Figure 8. (Color online) Best-fit circuit parameter values for the cell containing the yarn in an aqueous NaPF_6 solution: (a) Y_0 , (b) P , and (c) R_2 based on directly fitting the circuit in Fig. 5a and based on Eq. 3. (d) The gravimetric capacitance based on Eq. 4 compared to the gravimetric capacitance found by fitting the circuit in Fig. 5b.

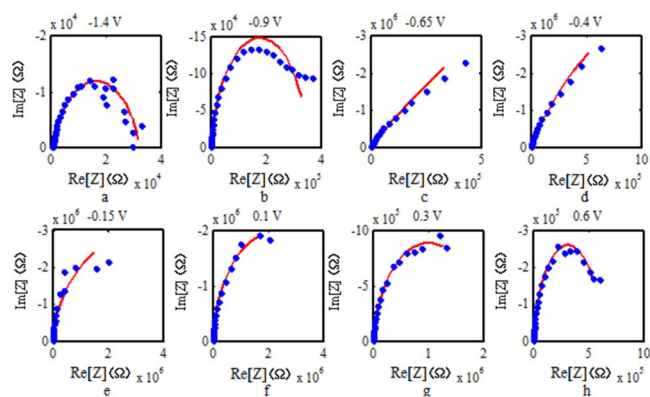


Figure 9. (Color online) Nyquist plots of the impedance of the MWNT yarn electrode in a 0.2 M solution of TBAPF_6 in acetonitrile at various potentials.

smaller, and the fitting uncertainty decreases significantly compared with the two aforementioned points, indicating that parasitic reactions start to happen at the WE. Figure 8b shows the dependence of the phase exponent P on bias potential. It can be seen that P varies only between 0.82 and 0.9. Figure 8d shows the gravimetric capacitance based on direct fitting of the circuit in Fig. 5b along with the value computed using Eq. 4 at the potentials where that equation is applicable.

Experiments in acetonitrile.— Similar measurements were performed in a 0.2 M solution of TBAPF_6 at various potentials ranging from -1.4 to $+0.6$ V vs Ag/Ag $^+$. The results of EIS measurements are plotted in Fig. 9. The circuit in Fig. 5a was fit to the impedance response, and the best-fit circuit parameter values are plotted as a function of the bias potential in Fig. 10. The simulated frequency responses of the best-fit circuits are shown along with the experimentally measured cell responses in Fig. 9. Figure 10b shows the dependence of the phase exponent P on bias potential. It can be seen that P varies only between 0.82 and 0.94. Figure 10d compares the capacitance found based on Eq. 4 and the best-fit capacitance value using the circuit in Fig. 5b. As can be seen in Fig. 10c, as was the

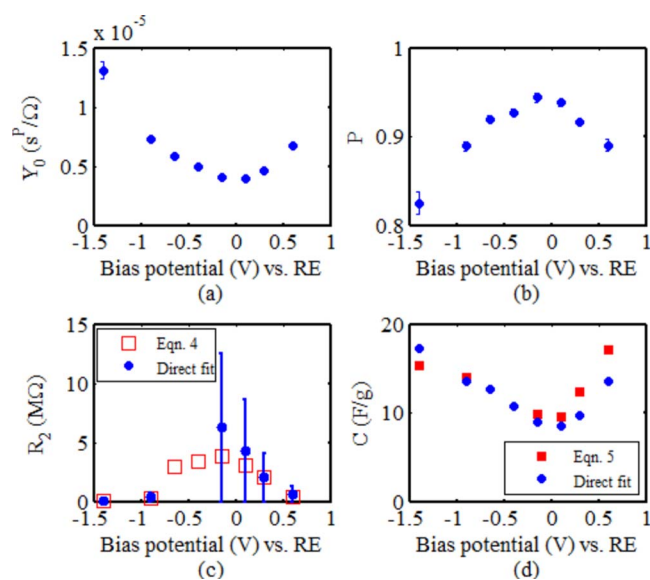


Figure 10. (Color online) Best-fit circuit parameter values for the cell containing the yarn in a solution of 0.2 M TBAPF_6 in acetonitrile: (a) Y_0 , (b) P , and (c) R_2 based on directly fitting the circuit in Fig. 5a and based on Eq. 3. (d) The gravimetric capacitance based on Eq. 4 compared to the gravimetric capacitance found by fitting the circuit in Fig. 5b.

case with the aqueous electrolyte, when the bias potential is not close to the extremes of the studied range, the fitting uncertainty for the parallel resistor R_2 becomes large, implying that this circuit parameter is irrelevant as no charge transfer should occur at low electrode potentials. The values of R_2 at those two points, that are deemed irrelevant, are not shown in Fig. 10c. At higher potentials, R_2 once again becomes much smaller and its fitting uncertainty decreases significantly compared to the two points mentioned above, indicating that parasitic reactions start to happen at the WE. Judging by the CV (Fig. 6b), reactions are significant above +0.5 and below -0.8 V. These numbers are once again consistent with breakdown potentials of water, implying that some water or moisture contamination must have entered the cell during the measurements. At potentials where Eq. 3 is applicable, the values found for R_2 are close to those obtained through direct fitting (squares). At $V = -0.65$ -0.4 V vs Ag/Ag⁺, the imaginary part of the impedance has no clear maximum, and hence Eq. 3 and 4 are not applicable.

Discussion.—Comparison between the plots in Fig. 8 and 10 shows that the gravimetric capacitance value in acetonitrile and water at low potentials is in the same range. However, while the gravimetric capacitance in the aqueous electrolyte is relatively independent of the bias potential, the gravimetric capacitance in acetonitrile seems to increase as the absolute value of the applied voltage is increased. One possible explanation is that the number of pores filled with electrolyte depends on potential because of the effect of charging on surface tension. Another possibility is the partial desolvation of ions as they enter into the pores of the yarn.²⁴⁻²⁶ In the process the ions get partially deprived of their solvation spheres at higher potentials, resulting in a smaller distance between the charge layer and the electrode surface and a higher capacitance. Small ions can penetrate deeper into the pores of the yarn, increasing the effective surface area. This is consistent with the observation of increased Y_0 at extreme potentials in acetonitrile (Fig. 10a). This increase in capacitance is not observed in the aqueous electrolyte. This may be because water molecules are smaller and more polar compared to acetonitrile, and therefore the solvation shell is not lost at potentials under study. It is also possible that the contaminating water in the acetonitrile electrolyte is partially contributing to the formation of solvation spheres, thus changing the capacitance of the Helmholtz layer in the acetonitrile electrolyte, making its size comparable to that of aqueous electrolyte. The estimated value of the capacitance from Eq. 4 is almost always larger than the value estimated by fitting the parallel-series RC circuit in Fig. 5b. Because the CPE provides a better fit than the RC circuit (whose fits are not shown here), the “real” capacitance value found from Eq. 4 is expected to be a better estimate of the capacitive behavior of the interface because it is based on a better fit.

In both model fits, the parallel resistor R_2 becomes irrelevant at smaller potentials, where no electron transfer is expected to take place across the electrode–electrolyte interface. The value of R_2 drops significantly as the potential difference across the electrode is increased and as charge starts to transfer through the interface. The solution of TBAP in acetonitrile is known to be stable over a large potential range of -2.9 to +3.4 V vs saturated calomel electrode (equivalent to about -3.26 to 3.04 V vs Ag/Ag⁺ 0.1 M).²⁷ Considering the potentials at which parasitic reactions occur according to the CV, it is likely that water (as a contaminant in the case of acetonitrile solvent) is the prime suspect for the parasitic reactions. The capacitive voltage range could be extended by employing anhydrous solvents. The electrochemical behavior of the yarn outside its purely capacitive range is still of great interest, because in electrochemomechanical actuators like this it is occasionally necessary to apply large potentials to the actuator,²⁸ and it is important to have electrochemical models that describe the behavior of the actuator at such potentials.²⁹

If the value of Y_0 is indeed related to the thickness of the double

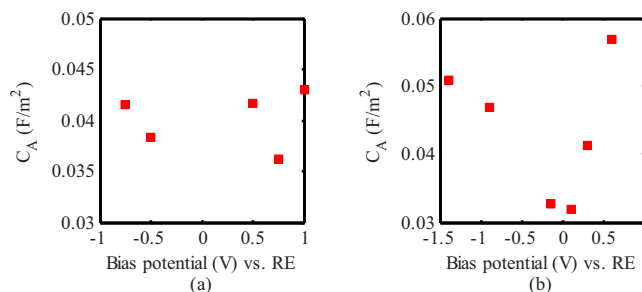


Figure 11. (Color online) Surface capacitance (F/m^2) of the MWNT bundles calculated based on the measured capacitances and the surface area of the bundles as modeled in Fig. 4: (a) in aqueous 1 M NaPF₆ and (b) in 0.2 M TBAPF₆ in acetonitrile.

layer, then it can be said that the double-layer thickness in the non-aqueous electrolyte changes more drastically compared to the aqueous electrolyte.

The phase exponent P has average values of about 0.88 in the aqueous electrolyte and about 0.89 in the nonaqueous electrolyte. The similarity of these two numbers supports our assumption that the CPE behavior is rooted in the structure of the MWNT yarn electrode. Based on the branched RC circuits discussed in Ref. 19, such an exponent can be explained by the existence of third level of branching. Indeed, if ions can diffuse between individual MWNTs in a bundle, a model employing a third level of branching physically justifies an exponent of 0.875, which is close to the estimated value.

The results for the gravimetric capacitance are consistent with the results found for CNT paper electrodes in acetonitrile by Barisci et al.¹¹ We did not observe a linear tail in the Nyquist plots at low frequencies as reported in Ref. 7 and 8, even though the lower frequency limit in our measurements was the same (0.01 Hz), except at 0 and 0.25 V in the aqueous electrolyte and at -0.65 and -0.4 V in the acetonitrile-based electrolyte. This may imply that electron-transfer effects dominate at the rest of the applied potentials in our measurements, a suggestion that is consistent with the parasitic currents evident in the CVs. The Nyquist plots in Ref. 9 are measured only at 1 V vs Pt in an ionic liquid, and it is therefore hard to compare the dependence of the behavior of their CNTs on the applied bias. Nevertheless, the larger phase angle of their electrodes implies a more capacitive behavior than that of our yarns, which is consistent with the CPE behavior in our yarns being determined by the self-similar structure of the yarns rather than the porous structure which is common in both materials.

Based on the magnitude of the current observed in the CV values, the capacitance in the acetonitrile electrolyte is about 17 F/g, which is consistent with the values of capacitance reported in Fig. 10d. Similarly, the capacitance of the yarn in the aqueous electrolyte is estimated using CV to be about 14 F/g, which is again quite close to the range of capacitances in Fig. 8d.

The capacitance per surface area of the bundles was calculated assuming that the yarn consists of parallel bundles of MWNTs with diameters of about 50 nm and using the capacitance values found above. The results for aqueous and acetonitrile-based electrolyte are plotted in Fig. 11. The estimated surface capacitance values are consistent with the range expected for MWNT sheets based on surface-area measurement (using Brunauer–Emmett–Teller³⁰).

Conclusions

The electrochemical response of a twist-spun yarn made of MWNTs was studied in aqueous and nonaqueous electrolytes using EIS and CV. The frequency dependence of the impedance of the yarn is found to comply with that of a model containing a CPE with a phase exponent close to 0.88, in parallel with a resistor modeling charge transfer across the interface. This parallel combination of the CPE and resistor is placed in series with another resistor, which can

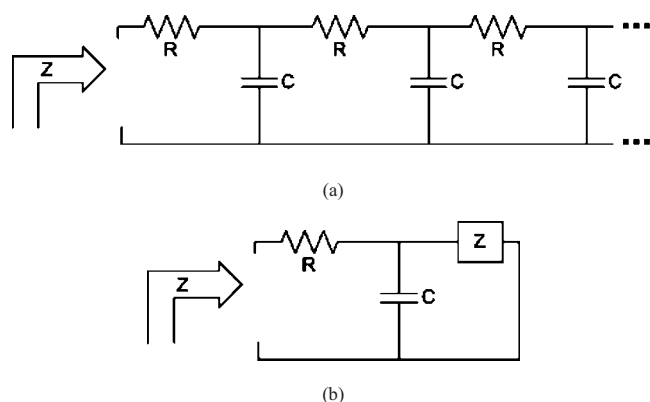


Figure A-1. (a) An infinite RC ladder network with the impedance Z and (b) its circuit equivalent.

model the solution and contact resistance. An attempt has been made to relate the exponent of the CPE to the physical structure of the yarn, which has a self-similar structure at length scales from 10 nm to 10 μm . Because the yarns show phase exponents of about 0.88, while similar MWNT structures with random orientations of nanotubes exhibit exponents closer to 1, it is possible that the CPE behavior of the yarns is related to nested transmission lines that are related to the underlying physical structure and to their self-similar (fractal) nature. The gravimetric capacitance of the yarn is estimated based on the CPE parameters. The capacitance per surface area of the MWNT bundles is estimated using the model, which is found to be consistent with previous reports.

University of British Columbia assisted in meeting the publication costs of this article.

Appendix

In order to find the input impedance of the infinite RC ladder circuit in Fig. A-1, we observe that this circuit can be redrawn as in Fig. A-1b. Based on the latter figure, the impedance can be easily determined as

$$Z = \frac{R}{2} \left(1 + \sqrt{1 + \frac{4}{j\omega CR}} \right) \quad [\text{A-1}]$$

Now let us assume that $R = R_0\Delta x$ and $C = C_0\Delta x$, where R_0 and C_0 are the resistance and capacitance per unit length of the material and Δx is a small length along the pore direction. Substituting Eq. A-1, we obtain

$$\begin{aligned} Z &= \frac{R_0\Delta x}{2} \left(1 + \sqrt{1 + \frac{4}{R_0C_0\Delta x^2j\omega}} \right) = \frac{R_0\Delta x}{2} + \sqrt{\left(\frac{R_0\Delta x}{2}\right)^2 + \left(\frac{R_0\Delta x}{2}\right)^2 \frac{4}{R_0C_0\Delta x^2j\omega}} \\ &= \frac{R_0\Delta x}{2} + \sqrt{\left(\frac{R_0\Delta x}{2}\right)^2 + \frac{R_0}{C_0j\omega}} \end{aligned} \quad [\text{A-2}]$$

In the limit, as $\Delta x \rightarrow 0$

$$\lim_{\Delta x \rightarrow 0} Z = \sqrt{\frac{R_0}{j\omega C_0}} \quad [\text{A-3}]$$

Therefore, the impedance of such an RC network can be calculated as

$$Z = \sqrt{\frac{R_0}{j\omega C_0}} \quad [\text{A-4}]$$

References

- R. H. Baughman, A. A. Zakhidov, and W. A. de Heer, *Science*, **297**, 787 (2002).
- M. Zhang, K. R. Atkinson, and R. H. Baughman, *Science*, **306**, 1358 (2004).
- T. Mirfakhrai, J. Oh, M. Kozlov, E. C. W. Fok, M. Zhang, S. Fang, R. H. Baughman, and J. D. W. Madden, *Smart Mater. Struct.*, **16**, S243 (2007).
- K. R. Atkinson, S. C. Hawkins, C. Huynh, C. Skourtis, J. Dai, M. Zhang, S. Fang, A. A. Zakhidov, S. B. Lee, A. E. Aliev, et al., *Physica B*, **394**, 339 (2007).
- T. Mirfakhrai, J. Oh, M. Kozlov, M. Zhang, S. Fang, R. H. Baughman, and J. D. Madden, *Advances in Science and Technology*, **61**, 65 (2008).
- T. Mirfakhrai, M. Kozlov, M. Zhang, S. Fang, R. H. Baughman, and J. D. W. Madden, in *Proceedings of SPIE Smart Materials and Structures/NDE*, SPIE, p. 6927081-8 (2008).
- Z.-H. Yang and H.-Q. Wu, *Chem. Phys. Lett.*, **343**, 235 (2001).
- Z.-H. Yang, S. Sang, Y. Feng, Y. Zhou, K. Huang, and H. Wu, *Diamond Relat. Mater.*, **14**, 1302 (2005).
- H. Zhang, G. Cao, Y. Yang, and Z. Gub, *J. Electrochem. Soc.*, **155**, K19 (2008).
- C.-M. Liu, H.-B. Cao, Y.-P. Li, H.-B. Xu, and Y. Zhang, *Carbon*, **44**, 2919 (2006).
- J. N. Barisci, G. G. Wallace, D. Chattopadhyay, F. Papadimitrakopoulos, and R. H. Baughman, *J. Electrochem. Soc.*, **150**, E409 (2003).
- R. de Levie, *Electrochim. Acta*, **10**, 113 (1965).
- C. H. Hsu and F. Mansfeld, *Corrosion (Houston)*, **57**, 747 (2001).
- R. de Levie, in *Advances in Electrochemistry and Electrochemical Engineering*, P. Delahay and C. W. Tobias, Editors, Interscience, New York (1967).
- J. R. Macdonald and W. R. Kenan, *Impedance Spectroscopy: Emphasizing Solid Materials and Systems*, Wiley-Interscience, New York (1987).
- A. Le Mehaute, *J. Stat. Phys.*, **36**, 665 (1984).
- A. Le Mehaute and G. Crepy, *Solid State Ionics*, **9-10**, 17 (1983).
- B. Sapoval and J.-N. Chazalviel, *Phys. Rev. A*, **38**, 5867 (1988).
- W. Scheider, *J. Phys. Chem.*, **79**, 127 (1975).
- R. Kant, R. Kumar, and V. K. Yadav, *J. Phys. Chem. C*, **112**, 4019 (2008).
- S. F. Mertens, C. Xhoffer, B. C. De Cooman, and E. Temmerman, *Corrosion (Houston)*, **53**, 381 (1997).
- F. Mansfeld and M. W. Kendig, *Mater. Corros.*, **50**, 475 (1999).
- T. Mirfakhrai, J. Oh, M. Kozlov, E. C. W. Fok, M. Zhang, S. Fang, R. H. Baughman, and J. D. Madden, *Adv. Sci. Technol. (Faenza, Italy)*, **61**, 65 (2008).
- J. Chmiola, G. Yushin, Y. Gogotsi, C. Portet, P. Simon, and P. L. Taberna, *Science*, **313**, 1760 (2006).
- R. Lin, P. L. Taberna, J. Chmiola, D. Guay, Y. Gogotsi, and P. Simon, *J. Electrochem. Soc.*, **156**, A7 (2009).
- P. Simon and Y. Gogotsi, *Nature Mater.*, **7**, 845 (2008).
- A. J. Fry, in *Laboratory Techniques in Electroanalytical Chemistry*, 2nd ed., P. T. Kissinger and W. R. Heineman, Editors, p. 469, CRC Press, Boca Raton, FL (1996).
- J. D. W. Madden, J. N. Barisci, P. A. Anquetil, G. M. Spinks, G. G. Wallace, R. H. Baughman, and I. W. Hunter, *Adv. Mater. (Weinheim, Ger.)*, **18**, 870 (2006).
- T. Mirfakhrai, M. Kozlov, M. Zhang, S. Fang, R. H. Baughman, and J. D. W. Madden, in *Proceedings of SPIE Smart Materials, and Structures/NDE*, SPIE, p. 65241H1-12 (2007).
- S. Shiraishi, M. Kibe, T. Yokoyama, H. Kurihara, N. Patel, A. Oya, Y. Kaburagi, and Y. Hishiyama, *Appl. Phys. A*, **82**, 585 (2006).